Comparison of Ti Si 1-x O 2 mixed oxide and TiO in SiO nanocomposite dielectric properties at nanoscale

Christina Villeneuve-Faure, M. Mitronika, Laurent Boudou, W Ravisy, M.P. Besland, Mireille Richard-Plouet, Antoine Goullet

Comparison of $Ti_xSi_{1-x}O_2$ mixed oxide and TiO_2 in SiO_2 nanocomposite dielectric properties at nanoscale

C. Villeneuve-Faure[1], M. Mitronika[2], L. Boudou[1], W. Ravisy[2], M.P. Besland[2], M. Richard-Plouet[2] and A. Goullet[2]

[1] LAPLACE, Université de Toulouse, CNRS, INPT, UPS, Toulouse, France,
[2] Nantes Université, CNRS, Institut des Matériaux de Nantes Jean Rouxel, IMN, F-44000 Nantes, France

***Abstract*- Thin dielectric films are involved in a lot of applications as MIM-capacitors. For this application, the target properties are high dielectric permittivity and low leakage current. To reach this goal, the relative merit of TiO_2/SiO_2-based mixed oxide and nanocomposite films is investigated in this paper. Results based on dielectric permittivity and current measurements at nanoscale emphasize a strong impact of dielectric films nano-structuration. Indeed, for the same level of current flowing through the dielectric layer, nanocomposite films exhibit a dielectric permittivity twice than the one of mixed oxide films. Moreover, the dielectric properties of the former are similar to those of classical high-k materials.**

I. INTRODUCTION

Concerning microelectronic applications, dielectric materials are used in a lot of passive or active devices. Among them, Metal-Insulator-Metal (MIM) capacitors are involved in a lot of applications such as analog-to-digital converters or dynamic random-access memory [1]. Considering MIM capacitor, SiO_2 thin films have interesting characteristics regarding high energy storage, but are limited by their low relative dielectric permittivity (ε_r) [2]. To overcome this drawback, the International Roadmap for Devices and Systems (IRDS) 2026 projection indicates a target of an equivalent oxide thickness (EOT) close to 1 nm, ε_r of at least 40 and a leakage current lower than 10^{-8} A.cm^{-2}. To reach the IRDS target, different approaches are developed. First, high-k materials, such as TiO_2, $BaTiO_3$ or Al_2O_3 appear interesting due to high relative dielectric permittivity but the main limitation is related to their high leakage current [1,3] and weak dielectric strength [4,5]. In this context, mixed oxides (MO) such as $Ti_xSi_{1-x}O_2$ appear attractive to take advantage of both SiO_2 low leakage current and of TiO_2 high ε_r. However, the ε_r increasing remains limited [6]. Another way of improvement deals with nanocomposite (NC) materials. Considering in Organic field-effect transistor (OFET), the use of thin polymer nanocomposite films based on TiO_2 or ZnO high-k nanoparticles (NPs) allows to improve performances in term of field-induced current [7]. However, a fully-inorganic NC material for MIM capacitors thin films are scarcely reported in the literature.

In this context, NC materials appear promising as they could combine advantages of each material. In this paper, we intend to compare TiO_2/SiO_2-based MO and NC films nanoscale dielectric properties in terms of leakage current and dielectric permittivity to identify the impact of nano-structuration.

II. EXPERIMENTS

A. Materials

The mixed oxide TiO_2-SiO_2 thin films (50 nm thick), were obtained by low-pressure PECVD technique in a home-made reactor. Oxygen (24 sccm) is introduced at the top of the plasma source and Ti or Si organometallic precursors are introduced by a distribution ring located at 8 cm above the substrate. More experimental details can be found in previous papers [8]. Titanium Tetra-Isopropoxide (TTIP) and Hexamethyl-disiloxane (HMDSO) vapors were used as Ti and Si precursors respectively. During the deposition, the pressure value (before plasma ignition) was set at 3 mTorr. The variation of the TTIP and HMDSO flow rate was used to vary the Ti content in the deposited TiO_2-SiO_2 mixed oxide films. By this way, we intended to elaborate $Ti_xSi_{1-x}O_2$ MO films with x = 0, 0.33, 0.49 and 0.54 [6].

The synthesis of TiO_2 in SiO_2 NC (50 nm thick) is based on the injection of a colloidal TiO_2 NPs solution in the PECVD reactor described above. Concomitantly, the deposition of the SiO_2 matrix is again ensured using HMDSO vapor and an O_2-based plasma. Prior injection, the colloidal solution dispersed in a propylene carbonate:propylene glycol (PC:PG) mixture needs to be diluted in a more volatile solvent in order to increase its volatility. Therefore, the final colloidal solution used was a mixture of PC:PG and methanol with a volume fraction of 20.25:54.75:25. The injection of the TiO_2 colloidal solution was achieved through a separate industrial direct-liquid dispenser (Kemstream). The injection operating in a pulsed regime, at a frequency of 0.5 Hz, is controlled by a valve whose orifice includes 8 holes with a diameter of 70 µm each. For maintaining very-low pressure during the deposition (3 mTorr) and therefore obtaining a high-quality inorganic matrix, the pulsed sequence was adjusted in order to manage periods without injection to recover the nominal pressure. Thus for a sequence of 1 min, we defined N (= 1, 10, 15, 20 and N_{max}=30) as the number of pulses lasting 1 ms that were triggered each 2s. Thus for N = 10 pulses, the dispenser valve is opened at a frequency of 0.5 Hz and after this first-time lapse of N × 2 s = 20 s (TON), the valve remains closed for 60-N × 2 s = 40 s (TOFF). Such sequence was repeated for 50 min. During this intermittent mode of injection, the oxygen

mass flow rate of the working gas was set at 24 sccm (standard cubic centimeters per minute) while the continuous mass flow rate of HMDSO vapor was maintained at 0.11 sccm. The fraction between HMDSO and O_2 was chosen in a way to produce a silica-like matrix with a very low carbon content. O_2 was also used to ensure the removal of solvent-based organic moieties surrounding TiO_2 NPs.
In addition, in both cases, the films and NC growth was monitored with in situ ellipsometry with real-time fitting, allowing to stop deposition when the targeted thickness (50 nm) was reached. Thickness values were obtained thanks to a robust fitting model, fully validated for higher thicknesses [6]. We are thus confident that the targeted thicknesses were achieved.

B. Structural characterization

The chemical composition analysis at the very surface of the films were performed by X-Ray Photoelectron Spectroscopy (XPS) on a Kratos Nova spectrometer with Al Kα radiation at 1486.6 eV. After wide range spectra in the 1200 to - 2 eV range in binding energy, high resolution spectra of relevant core level were recorded with charge neutralizer, i.e. O 1s, Ti 2p and Si 2p. The decomposition in elemental components and fitting of the measured peaks were carried out using CasaXPS software [9] and Gaussian-Lorentzian functions.
The surface morphology of the thin films was assessed using SEM and AFM with JEOL JSM 7600F in a secondary electron mode operating at 5 kV and with a Bruker Multimode 8 setup in tapping mode, respectively.
The Spectroscopic Ellipsometry (SE) measurements were conducted in the 245 nm to 1000 nm wavelength range at 71.7° incident angle using a rotating compensator ellipsometer (J.A. Woollam M-2000). The fitting was performed using CompleteEASE software using the Cauchy model for SiO_2, the Tauc Lorentz (TL) model for $Ti_xSi_{1-x}O_2$ and the Bruggeman effective medium approximation (BEMA) for NC (i.e. to model the TiO_2 NPs dispersed in the SiO_2 matrix).

C. Nanoscale dielectric properties characterization

Nanoscale electrical characterizations were performed on a Bruker Multimode 8 setup in Electrostatic Force Microscopy (EFM) mode for dielectric permittivity and Conductive AFM (C-AFM) for the current.

EFM phase shift ΔΦ measurements were done using 20 nm-lift and Pt-coated Si-tip with a quality factor Q of 293, a curvature radius Rc of 25 nm and a spring constant k of 2.81 $N.m^{-1}$. The phase shift parameter $a_{\Delta\Phi}$ is deduced [10]:

$$a_{\Delta\Phi} = [\Delta\Phi(V_1) - \Delta\Phi(V_2)]/[V_1^2 - V_2^2] \quad (1)$$

where $\Delta\Phi(V_i)$ is the phase shift measured with a bias voltage V_i applied on the tip. (i.e. 0V or 5V).

A three steps methodology was developped to extract the ε_r cartography from the measured frequency or phase shift parameter 11]. First, a 2D-axisymmetric finite element model on COMSOL Multiphysics® was used to compute in air and dielectric, the electric field distribution and the electrostatic force Fe on AFM-tip at various lift. Secondly, the second derivative of the capacitance between AFM-tip and dielectric sample d^2C / dz^2 was deduced from Fe. And finaly related phase shift parameter $a_{\Delta\Phi}$ was computed:

$$a_{\Delta\Phi} = [Q/(k)]\,[d^2C/dz^2] \quad (2)$$

By this way the theoretical relationship between phase shift $a_{\Delta\Phi}$ parameter and ε_r was obtained.

Current measurements at nanoscale were performed with a PtIr coated Si-tip (Rc = 27 nm and k = 0.4 $N.m^{-1}$) using the Conductive AFM (C-AFM) mode with low noise amplifier modules and low contact force (30 nN). Different bias voltage was applied to the films as a function of film conductivity. The current collection surface S_c is estimated to 2 10^{-3} μm².

III. RESULTS ANS DISCUSSION

A. Morphology and Structural characterization

To investigate the chemical composition of the TiO_2 in SiO_2 NC and of the $Ti_xSi_{1-x}O_2$ MO thin films, at the very surface, XPS measurements were carried out. Concerning MO, the results confirm that we manage to elaborated $Ti_xSi_{1-x}O_2$ films with a Ti atomic percentage of 0%, 33%, 49% and 54 % which correspond to x = 0, 0.33, 0.49 and 0.54 respectively [6]. Concerning NC, XPS results are reported in Table I and compare to those provided by the SE and the BEMA model concerning the volume fraction of TiO_2 NPs [12].

TABLE I.
Evolution of Ti content (at.% relatively to silicon) from XPS analyses and of TiO_2 volume fraction from SE as function of number of pulses N for TiO_2 in SiO_2 NC.

N	Ti content	TiO_2 volume fraction (%)
1	0.13	3.1
10	2.8	13.3
15	6.2	36.8
20	9.16	51
30	29.8	57

Fig. 1 compares the surface topography of MO and NC materials. Concerning the $Ti_xSi_{1-x}O_2$ films, the surface morphology is smooth and homogeneous (Fig. 1.a and 1.b) and weakly influenced by Ti contents. Indeed, the surface roughness remains constant around 0.45 ± 0.5 nm. Concerning NC films, the surface morphology depends strongly on the Ti contents. For low amount of TiO_2 NP (N ≤ 10), the surface topography is flat, with few circle-like shape structures (Fig.1.c) and surface roughness is close to SiO_2 one (around 0.55 nm). For high amount of TiO_2 NPs (N > 10), the surface topography presents a lot of circle-shape structures which could overlap (Fig. 1.d) which implies an increasing of the surface roughness of one order of magnitude (7.1 ± 0.5 nm). Such circle-shape structures are related to a coffee-ring effect, which could have occurred during the evaporation of aerosol droplet [12]. These results confirm the features that were already observed at the Scanning Electron Microscopy and Transmission Electron Microscopy scales as described in previous papers [12].

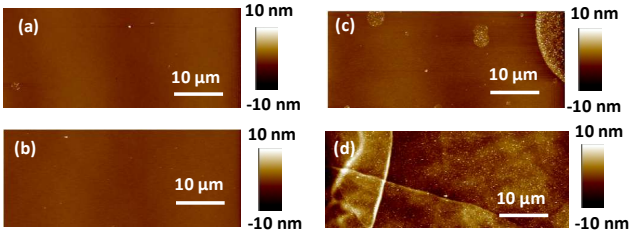

Fig. 1. Surface topography of (a) SiO_2, (b) $Ti_xSi_{1-x}O_2$ with x = 0.54, and TiO_2 in SiO_2 NC with number of pulses (c) N = 10 and (d) N = 30.

B. Dielectric properties

Fig.3 compares the surface topography and the ε_r map obtained by EFM on $Ti_xSi_{1-x}O_2$ MO and TiO_2 in SiO_2 NC materials. Concerning the SiO_2 layer, the surface topography is smooth (Fig. 3.a) and the ε_r map is homogeneous with a mean value of 3.7 which is closed to thermal silica one [13]. Concerning the $Ti_xSi_{1-x}O_2$ films with x = 0.33, the surface topography (Fig. 3.b) is similar to SiO_2 one. The ε_r map (Fig. 3.e) is homogeneous and the mean value is around 7 which is higher than SiO_2. For NC with a number of pulses N ≤ 10 (i.e. Ti contents less than 2.8%), the surface topography is smooth (Fig. 3.c) and the ε_r map is homogeneous but with a mean value higher than SiO_2 (results not shown). For N > 10, the surface topography presents a lot of grains (Fig. 3.c) which is consistent with the increase of the surface roughness. The corresponding ε_r map (Fig.4.f) is no more homogeneous and presents high ε_r area (orange/red) and low ε_r area (dark blue) which corresponds respectively to TiO_2-rich ($\varepsilon_r \approx$ 60-80) and SiO_2-rich ($\varepsilon_r \approx 3.8$) zones. As the lateral dimension of the TiO_2 NPs is around 4nm, the TiO_2-rich area corresponds to gathering of NPs . The main value of ε_r is around 29.5 for N = 30 (i.e. Ti contents of 29.8%).

Fig. 4 compares the evolution of the ε_r as function of the Ti contents provided by XPS for $Ti_xSi_{1-x}O_2$ MO and TiO_2 in SiO_2 NC. For both materials the ε_r increases with the Ti content. However, this increase is more important for NC than for MO. For a Ti content of around 30 at.%, the ε_r is equal to 7 for MO and to 29.5 for NC. This implies that the introduction of TiO_2 NPs in SiO_2 matrix is a more efficient process to increase ε_r.

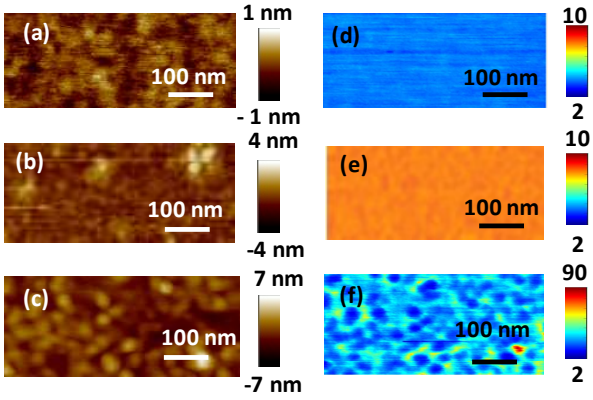

Fig. 3. (a-c) Surface topography and (d-f) ε_r map probed by EFM. (a, d) SiO_2, (b,e) $Ti_xSi_{1-x}O_2$ with x=33% and (c,f) TiO_2 in SiO_2 NC with 28.9% of Ti.

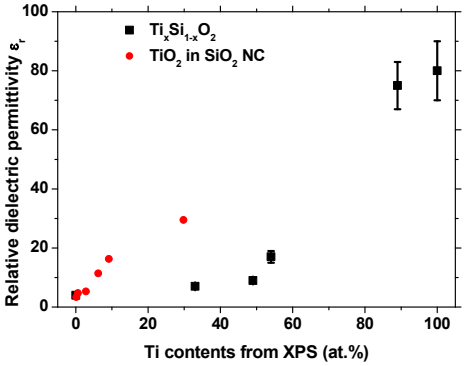

Fig.4. Evolution of the relative dielectric permittivity as function of Ti contents.

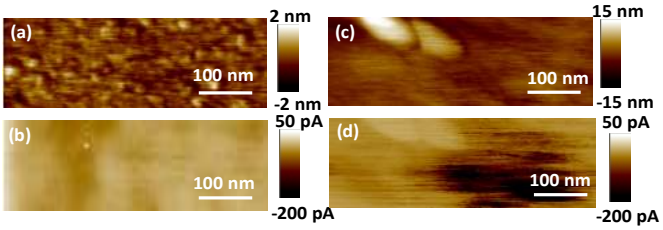

Fig.5. (a) Surface topography and (b) current map for -30V applied on $Ti_xSi_{1-x}O_2$ with x = 0.33. (d) Surface topography and (d) current map for -18 V applied on TiO_2 in SiO_2 NC with N = 30.

Fig. 5.a and 5.b compare the surface topography and the current map for -30 V applied on MO films with x = 0.33. The current is homogeneously distributed over the whole scanning area and a mean value of -80 pA was recorded. A homogeneous current map, with different mean value is observed for $Ti_xSi_{1-x}O_2$ with x ≥ 0.33. Fig. 5.c and 5.d compare the surface topography and current map for -18 V applied on TiO_2 in SiO_2 NC with N = 30. Similarly, to the ε_r map (Fig. 3.f), the current flowing through the NC films is not homogeneously distributed over the surface and 3 different areas are identified. (i) A low current area (white in Fig. 5.d), represents around 25% of the surface and exhibits a current ranging from -5 pA and -25 pA. This area corresponds to SiO_2-rich zone identified on ε_r map (Fig 3.f). (ii) A medium current area (light brown on Fig. 5.d), represents around 60% of the surface and exhibits a current ranging from -25 pA and -200 pA. (iii) A high current area (dark brown on Fig. 5.d) represents 15% of the surface and exhibits a current ranging from -100 pA to -600 pA. This area could be related to the presence of several TiO_2 NPs (i.e. high ε_r area on Fig. 4.f), as TiO_2 conductivity for electrons is important [12]. For NC with N = 20, only 10% of the surface is conductive (current around -20 pA for -28 V) and these areas should correspond to TiO_2-rich ones. For NC with N ≤ 20 no current was probed whatever the applied voltage value.

Fig. 6 compares the evolution of the C-AFM mean current over 1 µm x 1 µm surface as a function of the bias for MO and NC films. For a Ti amount of 30 at.%, the NC film (N = 30) presents a mean current two order of magnitude higher than MO. Thus, for a same amount of Ti, NC films present higher ε_r but equally higher current than MO.

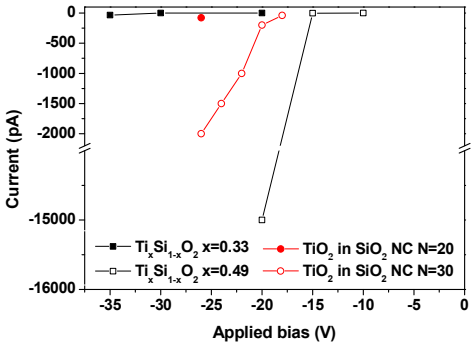

Fig. 6. Evolution of the mean value of the current probed by over the probed area (1 µm x 1 µm) as function of the applied bias.

Moreover, quite the same current is observed for N = 20 NC (i.e. 9.2% of Ti) and for $Ti_{0.33}Si_{0.67}O_2$ whereas the ε_r is higher for NC. As a consequence, for similar current, NC films appear to achieve higher ε_r than MO.

In Table II are gathered the dielectric properties of MO and NC films which could be considered as high-k material (i.e. ε_r > 10) [13]. Results highlight that, for similar ε_r, NC films exhibits lower current density J than MO. In term of ε_r our films are similar to classical high-k material, however it is rather difficult to compare C-AFM current density to macroscale one as the surface collection in C-AFM is low, difficult to determine accurately [14] and does not permit to reach very low current density (i.e. lower than 10^{-2} - 10^{-3} A.cm^{-2}). However, 60 nm-thick Y_2O_3 film processed by ALD exhibits a leakage current around 1 A.cm^{-2} which is close to the one of NC 9.16% of Ti with a comparable ε_r [15]. Similar conclusion could be done concerning the comparison of NC 29.8% of Ti and $LaAlO_3$ [16] which implies that TiO_2 in SiO_2 NC are competitive to replace high-k materials in MIM-capacitor. The next step is related to the improvement of TiO_2 NPs dispersion in the SiO_2 matrix to decrease the occurrence of TiO_2-rich areas and consequently the current.

TABLE II.

Comparison of ε_r, EOT (films thickness of 50nm) and leakage current density J at 25V (S_c = 2 10^{-3} µm²). High-k materials with similar ε_r [13].

	Ti (%)	ε_r	EOT (nm)	J (A/cm^{-2})	High-k material
NC	6.2	11	17.7	0	Al_2O_3, $HfSiO_4$
	9.16	17	11.5	8	Y_2O_3
	29.8	30	6.5	2 10^2	a-$LaAlO_3$
MO	54	18	12	45 10^2	Y_2O_3

IV. CONCLUSION

This paper emphasizes the difference in term of morphology and dielectric properties between TiO_2/SiO_2-based MO and NC films. $Ti_xSi_{1-x}O_2$ dielectric layers present homogeneous distribution of dielectric permittivity and current, whereas TiO_2 in SiO_2 NC films reveal heterogeneous dielectric properties mainly at high concentration in TiO_2 NPs (upper than 6% in volume). Indeed, observed TiO_2 rich areas exhibit high ε_r and current and correspond to gathering of TiO_2 NPs (3 maximum). Moreover, the influence of the Ti content is really different for MO and NC films as the same Ti content induces higher ε_r in NC that in MO. For capacitance applications, the scope of high dielectric permittivity and low leakage current is reached for a Ti content of 6.2 % for NC and for 33% for MO. Therefore, NC films should be more suitable for MIM capacitance applications than MO and their properties are competitive to high-k materials. Managing the coffee ring effect that may lead to some agglomerations of NPs is currently under progress as it can be counterbalanced by adjusting the solvent composition of the TiO_2 colloidal solution. Actually, this is also a way to tune the TiO_2 NPs concentration in solution and in the NCs. Consequently, improvement in terms of dielectric properties are to be expected, in the future.

ACKNOWLEDGMENT

This work was financially supported by the French GDR SEEDS.

REFERENCES

[1] M. Jenkins *et al.* "Review – beyond the highs and lows; a perspective on the future of dielectrics research for nanoelectronic devices". *ECS J. Solid State Sci. Technol.* Vol. 8, p.159, 2019

[2] B. Fan, F. Liu, G. Yang, H. Li, G. Zhang, S. Jiang and Q. Wang "Dielectric materials for high-temperature capacitors" *IET Nanodielectric* Vol. 1, pp.32-40, 2018

[3] W. Jeon "Recent advances in the understanding of high-k dielectric materials deposited by atomic layer deposition for dynamic random-access memory capacitor applications". *J. Mat. Res.* Vol. 35**,** pp.775-794, 2020

[4] K. Yim *et al.* "Novel high-k dielectrics for next-generation electronic devices screened by automated ab initio calculations" *NPG Asia Mater.* Vol. 7, e190, 2015

[5] M.S. Khan, H.J. Kim, T. Taniguchi, Y. Ebina, T. Sasaki and M. Osada "Layer-by-layer engineering of two-dimensional perovskite nanosheets for tailored microwave dielectrics". Appl. Phys. Express Vol. 10, p.091501, 2017

[6] M. Mitronika, C. Villeneuve-Faure, F. Massol, L. Boudou, W. Ravisy, M.P. Besland, A. Goullet and M. Richard-Plouet, "TiO_2-SiO_2 mixed oxide deposited by low pressure PECVD: insights on optical and nanoscale electrical properties", *Appl. Surf. Sc*. Vol. 541, p.148510, 2021

[7] F.C. Chen, C.W. Chu, J. He, and Y. Yang "Organic thin-film transistors with nanocomposite dielectric gate insulato". *Appl. Phys. Lett*. Vol. 85, p.3295, 2004

[8] D. Li, S. Elisabeth, A. Granier, M. Carette, A. Goullet and J.P. Landesman, "Structural and Optical Properties of PECVD TiO_2–SiO_2 Mixed Oxide Films for Optical Applications" *Plasma Processes and Polym.* Vol.13, p.918, 2016

[9] N. Fairley *et al.* "Systematic and collaborative approach to problem solving using X-ray photoelectron spectroscopy" *Appl. Surf. Sc. Adv.* Vol. 5, p.100112, 2021

[10] C. Riedel *et al.* "Determination of the nanoscale dielectric constant by means of a double pass method using electrostatic force microscopy" *J. Appl. Phys.* Vol. 106, p.024315, 2009

[11] M. Houssat, C. Villeneuve-Faure, N. Lahoud Dignat and J.-P. Cambronne "Nanoscale mechanical and electrical characterization of the interphase in polyimide/silicon nitride nanocomposites" *Nanotechnol.* Vol. 32, p.425703, 2021.

[12] M. Mitronika, J. Profili, A. Goullet, N. Gautier, N. Stephant, L. Stafford, A. Granier and M. Richard-Plouet, "TiO_2 –SiO_2 nanocomposite thin films deposited by direct liquid injection of colloidal solution in an O_2 /HMDSO low-pressure plasma". *J. Phys. D: Appl. Phys.* Vol. 54, p.085206, 2021

[13] J. Robertson "High dielectric constant oxides" *Eur. Phys. J. Appl. Phys.* Vol. 28, p.265, 2004

[14] F. Mortreuil, L. Boudou, K. Makasheva, G. Teyssedre and C. Villeneuve-Faure "Influence of dielectric layer thickness on charge injection, accumulation and transport phenomena in thin silicon oxynitride layers: a nanoscale study" *Nanotechnol.* Vol.32, p.065706, 2021

[15] H. Xu, X. Ding, J. Qi, X. Yang and J. Zhang "A Study on Solution-Processed Y_2O_3 Films Modified by Atomic Layer Deposition Al_2O_3 as Dielectrics in ZnO Thin Film Transistor" *Coatings* Vol. 11, p.969, 2021

[16] S. Pelloquin, *et al.* "$LaAlO_3$/Si capacitors: Comparison of different molecular beam deposition conditions and their impact on electrical properties" *J. Appl. Phys*. Vol. 113, p.034106, 2013